Kondo lattice model studied with the finite temperature Lanczos method

I. Zerec,[1] B. Schmidt,[2] and P. Thalmeier[2]
[1]*Max Planck Institute for the Physics of Complex Systems, D-01187 Dresden, Germany*
[2]*Max Planck Institute for Chemical Physics of Solids, D-01187 Dresden, Germany*
(Received 24 February 2006; published 16 June 2006)

We investigate the Kondo lattice model on two-dimensional (2D) clusters using the finite temperature Lanczos method. The temperature dependence of thermodynamic and correlations functions are systematically studied for various Kondo couplings J_K. The ground state value of the total local moment is presented as well. Finally, the phase diagrams of the finite clusters are constructed for periodic and open boundary conditions. For the two boundary conditions, two different regimes are found for small J_K/t, depending on the distribution of noninteracting conduction electron states. If there are states within J_K around the Fermi level, two energy scales, linear and quadratic in J_K, exist. The former is associated with the onsite screening and the latter with the RKKY interaction. If there are no states within J_K around the Fermi level, the only energy scale is that of the RKKY interaction. Our results imply that the form of the electron density of states (DOS) plays an important role in the competition between the Kondo screening and the RKKY interaction. The former is stronger if the DOS is larger around the Fermi level, while the latter is less sensitive to the form of the DOS.

DOI: 10.1103/PhysRevB.73.245108 PACS number(s): 62.30.+d, 65.40.−b, 66.35.+a

I. INTRODUCTION

The Kondo lattice model (KLM) is used to describe compounds containing localized magnetic moments, such as heavy fermion systems and Kondo insulators.[1] The KLM Hamiltonian is given by

$$H_{\mathrm{KL}} = -t\sum_{i,j;\sigma} c^{\dagger}_{i,\sigma}c_{j,\sigma} + J_{\mathrm{K}}\sum_{i} \boldsymbol{\tau}_i \cdot \mathbf{S}_i. \tag{1}$$

Here, $\boldsymbol{\tau}_i$ and $\mathbf{S}_i$ are itinerant and local (f) spins on site i, respectively. The KLM takes into account hopping of conduction electrons, t, and their Kondo interaction, J_K, with local f spins. The Kondo term causes a screening of local spins, but also induces indirect RKKY interactions between the local spins on the lattice. These two interactions compete, leading to either magnetically ordered or nonmagnetic ground states, separated by the quantum critical point (QCP).[2] The nature of the QCP in heavy fermion compounds is one of the central topics of condensed matter physics today.[3–10]

Various analytical and numerical methods have been used to study the KLM, like the mean-field approach[11] and Quantum Monte Carlo (QMC) method.[12] The finite temperature Lanczos method (FTLM)[13] has been used to study thermodynamic functions.[14] Also, the periodic Anderson model on finite size clusters has been studied with similar methods recently.[15]

Here, we use the FTLM and mainly focus the analysis on the temperature dependence and the ground state values of static correlation functions, of central importance for the QCP. We compare onsite versus intersite correlations on the lattice and also compare the former with the impurity case. The latter is associated with RKKY interactions. We also investigate the evolution of the total onsite moment with Kondo coupling strength J_K. The main advantage of the FTLM is that it involves no uncontrolled approximations and is exact for finite size clusters. It treats both Kondo screening and RKKY interactions, correctly.

We consider the eight-site cluster of a square lattice, as shown in the inset of Fig. 1, with periodic (PBC) and open (OBC) boundary conditions at half filling.

We will show that for this cluster the two different boundary conditions lead to two interesting physical situations, which may have relevance to the two types of QCP's observed (cf. Ref. 7 and references cited therein). There is, of course, only one solution of the KLM in the thermodynamic limit. However, the real materials have more complex band structures than described by the n.n. hopping in Eq. (1). By varying boundary conditions for the KLM on the small cluster, one may mimic band structures with a different characteristic behavior of the density of states (DOS) around the Fermi level. For this reason we present in detail the analysis of the KLM on the finite cluster for the PBC and the OBC and compare the two cases. In Sec. II we discuss the specific

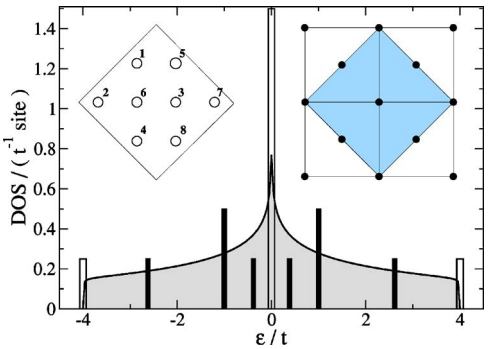

FIG. 1. (Color online) DOS for the tight-binding model in two dimensions is shown shaded. Unshaded bars represent discrete levels of the 2D eight-site cluster (for $J_K=0$) with PBC. The black bars represent levels with OBC. The bar heights correspond to the level degeneracy (divided by 8). Left inset: The eight-site cluster with site indices. Right inset: The first Brillouin zone with the k points corresponding to Bloch states of an eight-site cluster. The shaded part represents the Fermi volume for the half filled case. There are 6 degenerate states on the "Fermi surface" when the multiplicities are taken into account correctly.

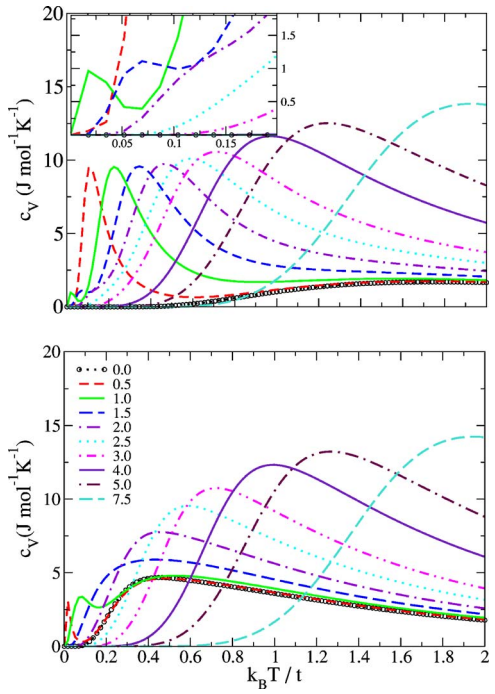

FIG. 2. (Color online) The specific heat calculated for various values of J_K/t, as indicated in the legend. The legend is valid for all the figures in this work, if not explicitly specified. Above: for PBC. The two low temperature peaks can be seen for $0.5<J_K/t\lesssim 2$. In the inset the lower peaks are magnified. Below: for OBC. The $J_K/t=0$ curve agrees well with the thermodynamic limit of the Hamiltonian (1). For $J_K/t>0$ there is only one low temperature peak.

heat anomalies obtained in the two cases. In Sec. III we discuss the central problem of Kondo-lattice physics: The competition and crossover behavior of onsite and intersite correlations as a function of temperature and control parameter J_K/t. The associated Kondo screening behavior evident from the susceptibility and total local moment is presented in Sec. IV. Finally, in Sec. V we summarize the results in a phase diagram and give the conclusions.

II. SPECIFIC HEAT

The specific heat for the PBC and the OBC, for various coupling constants J_K, is shown in Fig. 2.

The low-temperature specific heat for noninteracting case, $J_K=0$, with PBC deviates significantly from the thermodynamic limit. The reason is that six out of eight electrons are placed on the "Fermi surface," shown in the inset of Fig. 1; thus the ground state is highly degenerate. The specific heat for OBC is closer to the thermodynamic limit. The peak from the hopping term for $J_K=0$ is much more pronounced and at lower temperature, $T^{\mathrm{OBC}}_{\mathrm{max},0}$, for OBC than for PBC. The electronic states for OBC are no longer Bloch states, but the important point is that the electron energies are shifted from, and distributed below, the "Fermi level." The distribution of these discrete levels is such that it relatively well mimics the continuum DOS in the thermodynamic limit, as shown in Fig. 1.

The specific heat for PBC and OBC, when Kondo interaction is turned on, shows qualitatively different behavior in the weak coupling regime, $J_K/t\lesssim 2$, as shown in Fig. 2. For PBC, a double peak structure is observed at low temperatures for $0.5<J_K/t\lesssim 2$. We may denote the positions of the upper and lower peak by $T^{\mathrm{PBC}}_{\mathrm{max},1}$ and $T^{\mathrm{PBC}}_{\mathrm{max},2}$, respectively. For OBC only one low temperature peak appears at $T^{\mathrm{OBC}}_{\mathrm{max},1}$. The origin of these peaks are spin degrees of freedom, whose degeneracy is lifted by Kondo interaction. In the strong coupling limit there is only one peak in the specific heat, and it does not depend on the boundary conditions.

The specific heat for OBC agrees with the results obtained with the same method for the ten-site cluster with PBC in Ref. 14, as well as with the results obtained with the QMC in Ref. 12.

III. SPIN CORRELATION FUNCTIONS: ONSITE SINGLET FORMATION VERSUS RKKY INTERACTIONS

The nature of the specific heat peaks may be revealed by considering appropriate static correlation functions. We focus the analysis on the following two: $\langle \boldsymbol{\tau}_1\cdot\mathbf{S}_1\rangle$ is the onsite correlation function between local and itinerant spins, while $\langle \mathbf{S}_1\cdot\mathbf{S}_5\rangle$ is the intersite correlation function between local spins on neighboring sites for PBC. For OBC these are $\langle \boldsymbol{\tau}_3\cdot\mathbf{S}_3\rangle$ and $\langle \mathbf{S}_3\cdot\mathbf{S}_6\rangle$, i.e., the inner sites 3 and 6 are considered, because they are more representative than sites on the edges of the cluster (cf. Fig. 1).

A. Periodic boundary conditions

The onsite correlations, $\langle \boldsymbol{\tau}_1\cdot\mathbf{S}_1\rangle$, for PBC as function of temperature are shown in Fig. 3. They are also compared with the onsite correlations for the impurity case, where there is only one local spin, at site 1, on the eight-site cluster. In the weak coupling regime the onsite screening is decreased in the lattice, because there are less itinerant spins per local spin available for the screening.

The inflection points of the correlation functions, as function of temperature, indicate that the upper peak in the specific heat, at $T^{\mathrm{PBC}}_{\mathrm{max},1}$, corresponds to the formation of the onsite correlations, whereas the lower one, at $T^{\mathrm{PBC}}_{\mathrm{max},2}$, corresponds to the formation of the intersite correlations. The ground state ($T=0$ K) correlations for the PBC as a function of coupling strength J_K/t are shown in the inset of Fig. 4. It is seen that the onsite correlations are stronger than the intersite correlations for all J_K/t. Another characteristic is that $\langle \boldsymbol{\tau}_1\cdot\mathbf{S}_1\rangle$ jumps to the large absolute value as soon as J_K is turned on. This is a consequence of the degenerate itinerant degrees of freedom at the Fermi level for $J_K=0$. The free itinerant spins on the "Fermi level" screen the local spins onsite as soon as $J_K>0$; the ground state splits off and is characterized by finite $\langle \boldsymbol{\tau}_1\cdot\mathbf{S}_1\rangle$ correlations. The unscreened parts of the local spins form intersite correlations, $\langle \mathbf{S}_1\cdot\mathbf{S}_5\rangle$, below $T^{\mathrm{PBC}}_{\mathrm{max},2}$, due to the RKKY interaction. The magnitude of $\langle \mathbf{S}_1\cdot\mathbf{S}_5\rangle$ increases rapidly as J_K is turned on. Because of the very small energy scale (quadratic in J_K), convergence problems appear in the calculation of ground state $\langle \mathbf{S}_1\cdot\mathbf{S}_5\rangle$ correlations for $J_K/t<0.5$, and we were not able to deter-

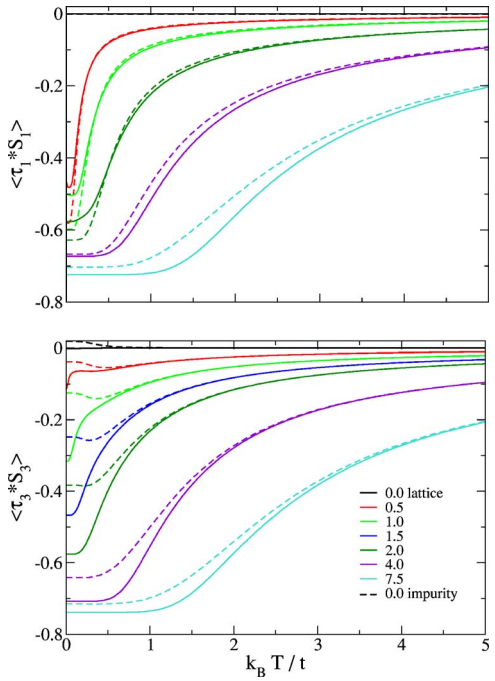

FIG. 3. (Color online) The onsite correlations in the lattice (full lines) as a function of temperature and the comparison with the impurity case (broken lines), for J_K/t values, as indicated in the legend. The correlation strength increases monotonically with increasing J_K/t. In the impurity case, the impurity local spin is placed on site 1 for the PBC, and site 3 for the OBC. Above: for PBC. Below: for OBC. Due to the small system size for the impurity case, there are some unphysical deviations at low temperatures and weak coupling J_K/t for the OBC.

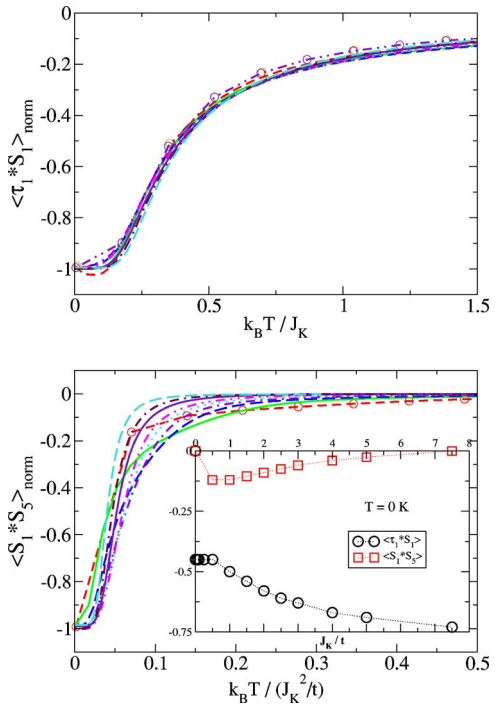

FIG. 4. (Color online) Correlation functions for PBC. Above: Normalized $\langle \boldsymbol{\tau}_1 \cdot \mathbf{S}_1 \rangle$ as function of temperature divided by J_K. Below: Normalized $\langle \mathbf{S}_1 \cdot \mathbf{S}_5 \rangle$ as a function of temperature divided by the square of J_K. The normalization is achieved by dividing the curves with the ground state values. In the inset the ground state (T=0 K) correlations as function of J_K/t are shown.

mine whether they also jump for finite J_K. In the strong coupling regime the intersite correlations vanish, while the onsite correlations saturate at $-3/4$, as the onsite singlets are formed.

The correlation functions, normalized to the ground state values, versus the scaled temperature, as done in Ref. 12, are shown in Fig. 4. The onsite correlations are characterized by a single temperature scale, perfectly linear in J_K/t. The intersite correlations are also characterized by a single temperature scale proportional to J_K^2/t. This shows that for PBC the onsite screening is independent of the intersite correlations, which may be associated with RKKY interactions. This is a consequence of the special symmetry of the eight-site cluster, which implies a large fraction of conduction electron sitting on the "Fermi surface." Nevertheless, it is an interesting result that may have relevance for a case where the conduction electron DOS is strongly peaked at the Fermi level.

B. Open boundary conditions

The onsite correlations, $\langle \boldsymbol{\tau}_3 \cdot \mathbf{S}_3 \rangle$, for OBC as a function of temperature and the comparison to the impurity case are also shown in Fig. 3. In contrast to the PBC, for OBC the onsite correlations are enhanced in the lattice. In the case of OBC there are no "free" itinerant spins, i.e., conduction electrons on the "Fermi level." In the weak coupling limit the onsite screening is not a direct process and is weak. The interesting point is the appearance of a new low energy scale in the lattice, which may be noted as a low-temperature downturn in the onsite correlations in Fig. 3.

The ground state correlations are shown in the inset of Fig. 5. The onsite correlations, $\langle \boldsymbol{\tau}_3 \cdot \mathbf{S}_3 \rangle$, do not jump as J_K is turned on, but rather increase continuously with J_K. The intersite correlations, $\langle \mathbf{S}_3 \cdot \mathbf{S}_6 \rangle$, are much stronger than $\langle \mathbf{S}_1 \cdot \mathbf{S}_5 \rangle$ for PBC, and in the weak coupling limit they are even larger in absolute values than the onsite $\langle \boldsymbol{\tau}_3 \cdot \mathbf{S}_3 \rangle$ correlations. It is understandable, because the local spins are only weakly screened, due to the lack of "free" itinerant spins. Therefore, the unscreened local spins can form strong intersite correlations.

The normalized correlations as function of the scaled temperature for OBC are shown in Fig. 5. The $\langle \boldsymbol{\tau}_3 \cdot \mathbf{S}_3 \rangle$ scale with J_K only in the strong coupling limit. In the weak coupling limit two characteristic temperatures or energy scales can be identified, as already mentioned previously. The upper one is associated with the energy splitting of the discrete energy levels (cf. Fig. 1), and is clearly a finite size effect. The lower energy scale is associated with the additional onsite screening, due to the presence of other local spins in the lattice. The intersite $\langle \mathbf{S}_3 \cdot \mathbf{S}_6 \rangle$ correlations are still approximately governed by a single energy scale, J_K^2/t, just as for PBC. Indeed the behavior of the normalized intersite correlation functions for OBC and PBC are quite similar, despite the fact that the magnitude differs by a factor of 2.

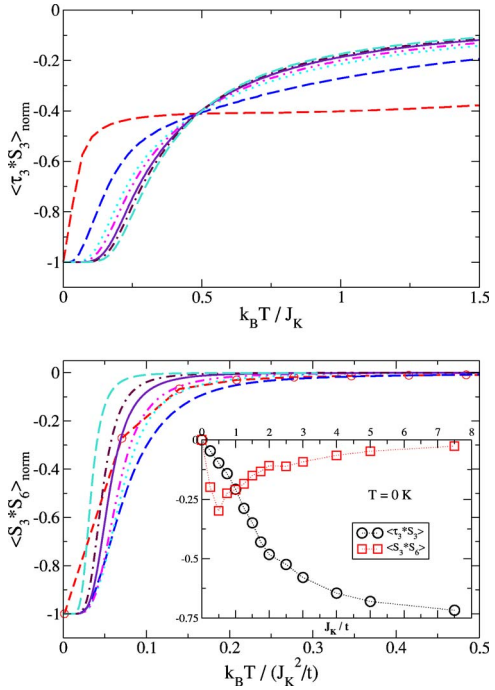

FIG. 5. (Color online) Correlation functions for OBC. Above: Normalized $\langle \boldsymbol{\tau}_3 \cdot \mathbf{S}_3 \rangle$ as a function of temperature divided by J_K. Below: Normalized $\langle \mathbf{S}_3 \cdot \mathbf{S}_6 \rangle$ as a function of temperature divided by $J_K{}^2/t$. The normalization is achieved by dividing the curves with the ground state values. In the inset the ground state ($T=0$ K) correlations as function of J_K/t are shown.

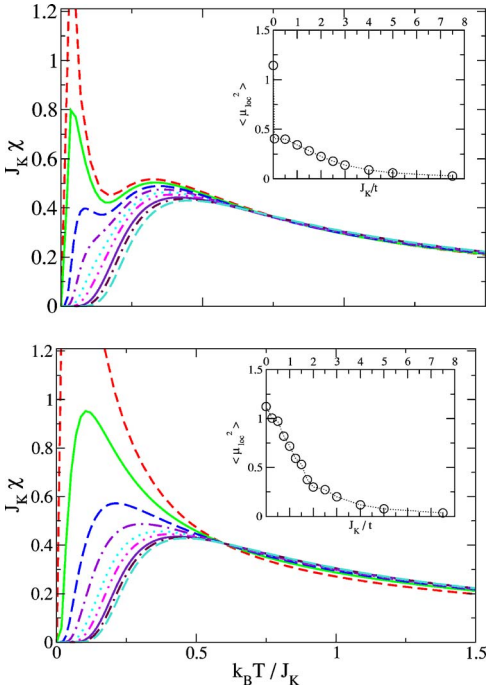

FIG. 6. (Color online) The scaled magnetic susceptibility, as indicated on the axes. Above: for PBC. Below: for OBC. In the insets the total local moments in the ground state (at $T=0$ K) as a function of J_K/t are shown, $\langle \boldsymbol{\mu}_{loc}^2 \rangle = \langle (\boldsymbol{\tau}_i + \mathbf{S}_i)^2 \rangle$ ($i=1,3$ for the PBC and OBC, respectively).

IV. MAGNETIC SUSCEPTIBILITY AND TOTAL LOCAL MAGNETIC MOMENT

The spin correlations are also directly reflected in the magnetic susceptibility, shown in Fig. 6, for PBC and OBC. It is multiplied by J_K and plotted versus temperature scaled with J_K, as was done in Ref. 12. The two peaks for PBC are clearly seen for small J_K/t, as in the specific heat. However, in the magnetic susceptibility even the lower peak for $J_K/t = 0.5$ is clearly seen. This is because the lower peaks in the magnetic susceptibility are much more pronounced and at slightly higher temperatures than the corresponding peaks in the specific heat. The position of the lower peak scales well with J_K^2 (not shown in the figure). The lower peak is not distinguishable anymore for $J_K/t \gtrsim 2$. The position of the higher peak scales with J_K. For OBC only one large peak is seen. For $J_K/t \lesssim 2$ it scales approximately with J_K^2. In the strong coupling limit, $J_K/t \gtrsim 2$, the peak scales linearly with J_K, just as for PBC. The results for OBC are similar to the results for the ten-site cluster with PBC in Ref. 14. These results are also similar to the results of the QMC calculations for larger clusters in Ref. 12. However, in Ref. 12, the magnetic susceptibility peak scales with $J_K{}^2$, while in the onsite correlations the characteristic temperature is proportional to J_K, suggesting the existence of two low energy scales.

In the insets of Fig. 6 the ground state values of the total local moments are shown, defined as

$$\langle \boldsymbol{\mu}_{loc}^2 \rangle = \langle (\boldsymbol{\tau}_i + \mathbf{S}_i)^2 \rangle = \langle \boldsymbol{\tau}_i^2 \rangle + \langle \mathbf{S}_i^2 \rangle + 2 \langle \boldsymbol{\tau}_i \cdot \mathbf{S}_i \rangle. \quad (2)$$

The interesting quantity here is $\langle \boldsymbol{\tau}_i^2 \rangle$, which is a measure of the itinerant spin localization. In the strong coupling limit $\langle \boldsymbol{\tau}_i^2 \rangle = 3/4$, i.e., the itinerant spins become localized as the onsite singlets are formed and the hopping of conduction electrons is frozen. When the conduction electrons are completely delocalized, i.e., for $J_K=0$, $\langle \boldsymbol{\tau}_i^2 \rangle = 3/8$, because the probability of finding one electron with spin up or down on one particular site is 1/2. Accordingly, $\langle \boldsymbol{\mu}_{loc}^2 \rangle = \langle \boldsymbol{\mu}_{loc}^2 \rangle_0 = 9/8$ for $J_K=0$ while for $J_K \to \infty$ it vanishes, as the onsite singlets are formed and the local moments completely screened. There is a jump for $J_K/t > 0$ for PBC. It has the same origin as the jump for the onsite correlations $\langle \boldsymbol{\tau}_1 \cdot \mathbf{S}_1 \rangle$, i.e., the highly degenerate unperturbed conduction electron ground state. A jump is also present in $\langle \boldsymbol{\tau}_i^2 \rangle$. For OBC we see a continuous decrease of $\langle \boldsymbol{\mu}_{loc}^2 \rangle$.

The $\langle \boldsymbol{\mu}_{loc}^2 \rangle$ is a good quantity to define a critical value of J_K/t at which the crossover from the predominantly magnetic to predominantly nonmagnetic ground state occurs. The other possibility would be to compare directly the intersite and onsite correlations, but the intersite correlations depend strongly on the cluster size. Therefore we define a critical $(J_K/t)_C$ as the value for which $\langle \mu_{loc}^2 \rangle = \langle \mu_{loc}^2 \rangle_0 / 2$. Then for OBC, $(J_K/t)_C \approx 1.4$ (cf. Fig. 6), in good agreement with the values obtained from the Quantum Monte Carlo[12] and the mean-field analysis.[16] For PBC it would be 0, but for this small cluster size, OBC are much more representative for the thermodynamic limit of the KLM.

V. PHASE DIAGRAM AND CONCLUSIONS

We may summarize the results in form of phase diagrams for PBC and OBC, shown in Fig. 7. In the phase diagrams

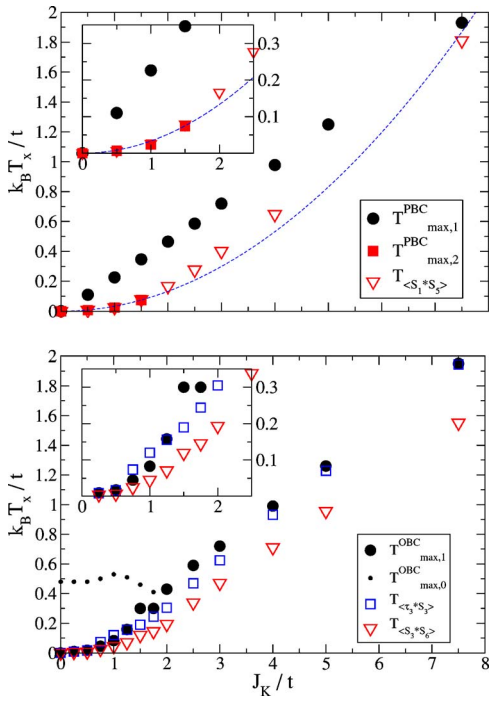

FIG. 7. (Color online) The phase diagrams for the eight-site 2D clusters. In the insets the weak coupling region is magnified. Above: for PBC. The inflection points are approximately determined as the temperatures where the normalized $\langle \mathbf{S}_1 \cdot \mathbf{S}_5 \rangle$ has the value of −0.75. The dashed line is the fitting curve assuming quadratic dependence on J_K. The inflection points of the onsite correlations agree with the positions of the upper peak in the specific heat and are not shown in the figure. Below: for OBC. The inflection points are approximately determined as the temperatures where the normalized correlation functions achieve the values of −0.8 and −0.75 for $\langle \boldsymbol{\tau}_3 \cdot \mathbf{S}_3 \rangle$ and $\langle \mathbf{S}_3 \cdot \mathbf{S}_6 \rangle$, respectively.

the positions of specific heat maxima are plotted as a function of coupling strength, J_K/t. Also, the inflection points of the correlation functions are plotted, and they mostly follow the positions of the corresponding specific heat maxima.

In the weak coupling regime, for PBC, two characteristic temperatures, $T^{\mathrm{PBC}}_{\mathrm{max},1}$ and $T^{\mathrm{PBC}}_{\mathrm{max},2}$, are found. The $T^{\mathrm{PBC}}_{\mathrm{max},2}$ cannot be determined for $J_K/t \gtrsim 2$, but we make the continuation with the $\langle \mathbf{S}_1 \cdot \mathbf{S}_5 \rangle$ inflection point temperature, $T_{\langle \mathbf{S}_1 \cdot \mathbf{S}_5 \rangle}$, which can be defined for all coupling strengths. Therefore we conclude that the corresponding anomaly in the specific heat is still there, but is too small to be identified. The inflection points of the correlation functions reveal that the characteristic temperatures $T^{\mathrm{PBC}}_{\mathrm{max},1}$ and $T^{\mathrm{PBC}}_{\mathrm{max},2}$ correspond to the energy scales of onsite correlations and intersite correlations, respectively. The former is linear in J_K for all J_K/t. The latter is proportional to ${J_K}^2/t$, and may be associated with the RKKY interaction.

For OBC, there is only one characteristic temperature, $T^{\mathrm{OBC}}_{\mathrm{max},1}$, for all J_K/t. In the weak coupling regime, for $J_K/t \lesssim 2$, below $T^{\mathrm{OBC}}_{\mathrm{max},1}$ predominantly intersite correlations are formed. However, $T^{\mathrm{OBC}}_{\mathrm{max},1}$ is also the characteristic temperature of onsite correlations. This is seen from the positions of inflection points for the corresponding correlations, also shown in the lower part of Fig. 7. Because the intersite correlations dominate and the characteristic temperature is approximately quadratic in J_K, the corresponding energy scale, in the weak coupling regime, may be associated with the RKKY interaction.

It is important to note that $T^{\mathrm{OBC}}_{\mathrm{max},1} \approx T^{\mathrm{PBC}}_{\mathrm{max},2}$, i.e., the RKKY interaction is not very sensitive to the distribution of noninteracting conduction electron states. This is plausible with the known expression for the RKKY characteristic temperature, $T_{\mathrm{RKKY}} \propto J_K^2/W$ (e.g., Ref. 4), where W is the bandwidth. It is also important that the RKKY energy scale is the energy scale of the onsite correlations in the weak coupling regime for the OBC. We may generally conclude that the RKKY energy scale is the lowest energy scale of the KLM; if the local spins are not screened above T_{RKKY}, then it is the only energy scale of the system.

In contrast, the onsite correlations, i.e., the onsite screening of local spins, is very sensitive to the number of states within J_K around the "Fermi level," as seen from the difference between $T^{\mathrm{PBC}}_{\mathrm{max},1}$ and for PBC and OBC, respectively. This is plausible with the expression for the single impurity Kondo temperature, which depends exponentially on the DOS at the Fermi level, $\rho(\epsilon_F)$; $T_K = \epsilon_F \exp\{-1/[J\rho(\epsilon_F)]\}$.

In the strong coupling regime, only one characteristic temperature is found for both PBC and OBC. It corresponds to the energy of the onsite singlet formation, which is linear in J_K. Boundary conditions are unimportant, because the local physics determines the properties of the system.

We may argue on the relevance of these results for the system in the thermodynamic limit. Recently a QCP was found[5,6,8] whose properties deviate from the expected behavior (e.g., Refs. 9 and 10). The properties of the system at the QCP are determined by the competition between the onsite screening and the RKKY interaction. Here we have shown that the competition between the onsite screening and the RKKY interaction strongly depends on the particular form of the distribution of noninteracting conduction electron levels. We may anticipate that in the thermodynamic limit this means a strong dependence on the particular form of noninteracting conduction electron DOS. A strongly peaked DOS near the Fermi level favors onsite screening, while the RKKY interaction is not very sensitive to the particular shape of the DOS. These results indicate that the shape of the DOS is very important for the properties of the heavy fermion systems in the vicinity of the QCP.

Finally, the qualitative behavior of the correlation functions for the KLM with OBC is similar to the KLM without charge degrees of freedom,[17] which is a generalized Kondo necklace model in 2D from Doniach's original work.[2] This shows that this simplified model describes well the spin degrees of freedom in the KLM at half-filling.

ACKNOWLEDGMENTS

We wish to acknowledge useful discussions with P. Fulde, S. Burdin, N. Perkins, and R. Ramazashvili.

[1] H. Tsunetsugu, M. Sigrist, and K. Ueda, Rev. Mod. Phys. **69**, 809 (1997).
[2] S. Doniach, Physica B & C **91**, 231 (1977).
[3] J. Rech, P. Coleman, G. Zarand, and O. Parcollet, Phys. Rev. Lett. **96**, 016601 (2006).
[4] P. Sun and G. Kotliar, Phys. Rev. Lett. **95**, 016402 (2005).
[5] S. Paschen, T. Lühmann, S. Wirth, P. Gegenwart, O. Trovarelli, C. Geibel, F. Steglich, P. Coleman, and Q. Si, Nature **432**, 881 (2004).
[6] J. Custers, P. Gegenwart, H. Wilhelm, K. Neumeier, Y. Tokiwa, O. Trovarelli, C. Geibel, F. Steglich, C. Pepin, and P. Coleman, Nature **424**, 524 (2003).
[7] Q. Si, S. Rabello, K. Ingersent, and J. Smith, Nature **413**, 804 (2001).
[8] A. Schröder, G. Aeppli, R. Coldea, M. Adams, O. Stockert, H. Löhneysen, E. Bucher, R. Ramazashvili, and P. Coleman, Nature **407**, 351 (2000).
[9] N. Mathur, F. Grosche, S. Julian, I. Walker, D. Freye, R. Haselwimmer, and G. Lonzarich, Nature **394**, 39 (1998).
[10] F. Steglich, B. Buschinger, P. Gegenwart, M. Lohmann, R. Helfrich, C. Langhammer, P. Hellmann, L. Donnevert, S. Thomas, A. Link, C. Geibel, M. Lang, G. Sparn, and W. Assmus, J. Phys.: Condens. Matter **8**, 9909 (1996).
[11] G.-M. Zhang and L. Yu, Phys. Rev. B **62**, 76 (2000).
[12] S. Capponi and F. F. Assaad, Phys. Rev. B **63**, 155114 (2001).
[13] J. Jaklic and P. Prelovsek, Adv. Phys. **49**, 1 (2000).
[14] K. Haule, J. Bonca, and P. Prelovsek, Phys. Rev. B **61**, 2482 (2000).
[15] Y. Luo, C. Verdozzi, and N. Kioussis, Phys. Rev. B **71**, 033304 (2005).
[16] G.-M. Zhang, Q. Gu, and L. Yu, Phys. Rev. B **62**, 69 (2000).
[17] I. Zerec, B. Schmidt, and P. Thalmeier, Physica B **378**, 702 (2006).